ACS APPLIED ELECTRONIC MATERIALS

pubs.acs.org/acsaelm Letter

Microstructuring GaAs Using Reverse-Patterning Lithography: Implications for Transistors and Solar Cells

Tianlang Yu, Devendra Khatiwada, Sahil Sharma, Maria D. Marquez, Venkat Selvamanickam,* and T. Randall Lee*

Cite This: ACS Appl. Electron. Mater. 2021, 3, 170−175 Read Online

ACCESS | Metrics & More | Article Recommendations | Supporting Information

ABSTRACT: This paper introduces reverse patterning lithography (RPL), which combines microcontact printing (μCP) of a custom-designed fluorinated adsorbate on gallium arsenide (GaAs) and the deposition of a polymeric resin as a wet-etching resist. Positive patterns were formed on GaAs wafers having various designed shapes and sharp edges at a lateral resolution of 100.0 μm and a depth of up to 3.0 μm. The RPL method benefits from being cost-effective and time-efficient compared to conventional photolithography and has the potential for use in the fabrication of various GaAs devices, including solar cells, light-emitting diodes, and microwave and radio frequency transistors.

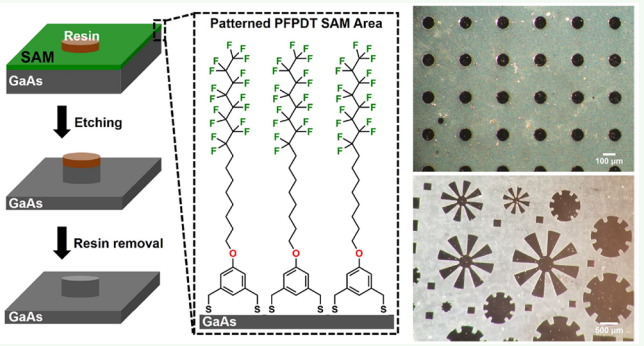

KEYWORDS: *reverse patterning lithography, patterned GaAs, microcontact printing, microstructuring, self-assembled monolayers, SAMs*

Gallium arsenide (GaAs) is an important III−V compound used in applications that require precise and/or demanding properties, such as photovoltaics (PVs) and microwave and radio frequency (RF) transistors. Although more costly than other semiconductors (e.g., silicon), GaAs exhibits low resistance, low off capacitance, high linearity at high frequencies, high electron mobility, and a direct bandgap.[1,2] The high electron mobility allows GaAs transistors to function at much higher frequencies than Si-based devices in RF applications.[3] Moreover, GaAs offers outstanding photovoltaic performance due to its direct bandgap.[4] For example, compared to Si-based materials, GaAs-based photovoltaic solar cells have been found to exhibit record-breaking conversion efficiencies, such as ∼29% for single-junction cells.[5] In RF applications, higher electron mobility allows GaAs amplifiers to function at much higher frequencies than Si-based devices.[6] Moreover, because of the widespread use of 4G networks and the current deployment of 5G, power amplifier modules in cell phones have also began to implement GaAs as the semiconductor of choice.[7] However, processing GaAs substrates to fabricate devices is difficult as well as costly and requires numerous lithographic steps.[8,9]

Conventional methods used for the fabrication of microelectronic devices include photolithography,[10] thermal nanoimprint lithography (T-NIL),[11] and UV-based nanoimprint lithography (UV-NIL).[12] The former method requires an expensive photoresist and photomask aligner. Conversely, the latter two methods require plasma treatment or reactive ion etching to remove the residual layer of the polymer resist used prior to the imprinting step.[13] In an effort to simplify the fabrication of GaAs-based devices, we have developed a cost-efficient method in which the combination of a microcontact printed (μCP) self-assembled monolayer (SAM) and a polymeric resin as a wet-etching resist was used to microstructure GaAs substrates. The new method, hereafter termed "reverse patterning lithography" (RPL; Scheme 1), takes advantage of the ability of the sulfur of *n*-alkanethiols to bind to GaAs surfaces to form nanoscale monolayer coatings that are poorly wettable and can be tuned to be antiadhesive.[14,15]

Extensive research conducted by the Lee group on SAMs generated on Au surfaces has shown enhanced thermal and chemical stability for films generated from bidentate adsorbates, when compared to the monodentate counterparts, due to the "chelate effect".[16−18] Furthermore, fluorinated materials, such as fluoropolymers and SAMs, have been shown to exhibit low surface energies, inertness, and high hydrophobicity as well as oleophobicity compared to their hydrocarbon counterparts.[19] To leverage the enhanced stability of the bidentate headgroup and the hydrophobic and oleophobic nature of fluorocarbons, we designed and

Received: October 5, 2020
Accepted: December 5, 2020
Published: December 21, 2020

Scheme 1. Illustration of Reverse Patterning Lithography for Microstructuring GaAs Substrates

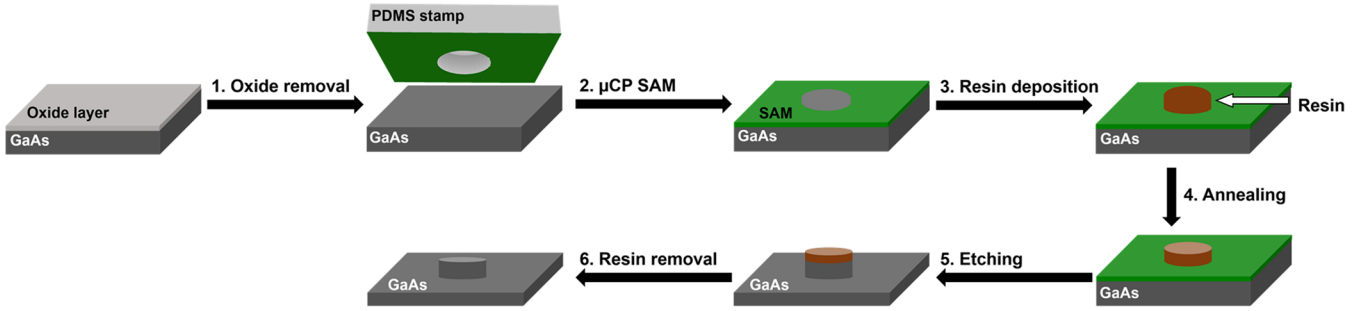

synthesized the fluorinated adsorbate, (5-(9,9,10,10,11,11,12,12,13,13,14,14,15,15,16,16,16-heptadecafluorohexadecyloxy)-1,3-phenylene)dimethanethiol (PFPDT), shown in Scheme 2, for use as an ink for patterning via microcontact printing (μCP).[20] The μCP process generates a hydrophobic and oleophobic thin film on selective areas of the GaAs substrate, which leads to microstructuring of GaAs in the RPL process (see Scheme 2).

Scheme 2. Illustration of Bidentate Fluorinated (5-(9,9,10,10,11,11,12,12,13,13,14,14,15,15,16,16,16-Heptadecafluorohexadecyloxy)-1,3-phenylene)dimethanethiol (PFPDT) for μCP of GaAs Substrates

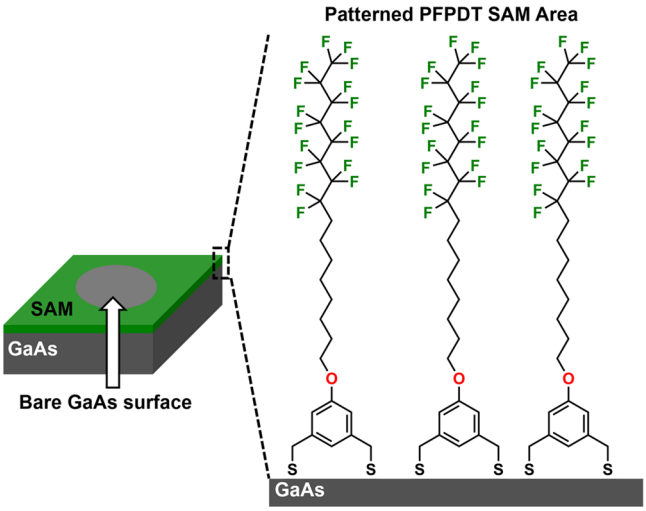

As noted above, Scheme 1 illustrates the overall RPL method, where microstructuring of GaAs single crystal substrates can be achieved in six steps. The first step in the RPL method involves removal of the native oxide layer atop the GaAs(100) wafer via submersion in ammonia solution (15% w/w) for 5 min followed by submersion into an HCl solution (15% w/w) for an additional 5 min with a water-rinsing step prior to introduction of the substrate into the HCl solution. After removal of the oxide layer, the fluorinated SAM was printed onto the freshly cleaned GaAs surface by using a PDMS stamp for 60 s (step 2, Scheme 1). The PDMS stamp was saturated with a 1 mM PFPDT solution in EtOH followed by drying the stamp with a flow of nitrogen. After formation of the hydrophobic pattern, the patterned GaAs surface was dipped into a resin solution made of 10% w/w phenolic resin in methoxypropyl acetate and then pulled out immediately to form a "reverse" resin pattern (step 3, Scheme 1). Note that the resin only covers the bare hydrophilic GaAs area, whereas the hydrophobic PFPDT SAM-covered areas remain uncoated. The GaAs sample was then annealed at 120 °C for 5 min to form a hard resin pattern with a thickness of ~0.20 μm at the center (step 4, Scheme 1). After annealing, the GaAs sample was placed into an etching solution (H_2O:H_2O_2:H_2SO_4 = 280:8:1 volume) for 10 min to form the designed pattern (step 5, Scheme 1). The final step of the process involves the removal of the resin by washing the GaAs substrate with acetone.

Analysis of PFPDT SAM Composition on GaAs Using XPS. To confirm the presence of the monolayer, the GaAs substrates were subjected to elemental analysis using X-ray photoelectron spectroscopy (XPS). Figure 1 shows the XPS spectra of the Ga 3d, As 3d, C 1s, F 1s, S 2p, and O 1s binding regions of the bare GaAs and PFPDT-printed GaAs after 30 min of ambient exposure, and Table 1 lists the assigned peaks along with their binding energies; peak assignments were based on examples found in the literature.[21−27] The Ga 3d binding energy region of both substrates exhibits a peak at 19.3 eV (Figure 1A). Because of a spin−orbit splitting of only 0.43 eV, the Ga $3d_{3/2}$ and Ga $3d_{5/2}$ peaks are indistinct and appear as a single peak. Furthermore, the bare GaAs (stored in ambient conditions) produces a native oxide layer, Ga_2O_3, which appears as a shoulder at 20.6 eV, overlapping with the GaAs peak. While acknowledging that the sensitivity to Ga and As oxides is typically low using laboratory X-ray sources, we note that the PFPDT-printed GaAs sample (blue line plotted in Figure 1A) fails to exhibit a shoulder associated with the oxide, suggesting not only the removal of the oxide layer upon treatment with PFPDT but also protection from oxidation of the surface under the limits of detection for at least 30 min of ambient exposure.[26]

Similarly, the As 3d binding energy region (Figure 1B) produced a single peak due to the small spin−orbit splitting of 0.69 eV for the As $3d_{3/2}$ and As $3d_{5/2}$ peaks at 41.1 eV. We also note the presence of arsenic oxides, As_2O_3 and As_3O_5, corresponding to the peak at ~43.0 eV; in contrast, in the spectrum of the PFPDT-printed surface there is no oxide peak (blue line plotted in Figure 1B). As noted for the Ga 3d spectra, the As 3d spectra of the PFPDT SAM protects the GaAs surface from oxidation for at least 30 min under ambient conditions. The presence of the oxides is also apparent in the O 1s spectrum of the bare GaAs surface (Figure 1C), with a sharp peak at 531.9 eV, while a markedly less pronounced peak is weakly noticeable in the PFPDT-printed surface. Note that the peak at 532.7 eV in the spectrum of the PFPDT-printed surface arises from the oxygen atom connected to the phenyl ring. As for the F 1s region (Figure 1D), only the PFPDT-printed surface produces a prominent peak at 688.9 eV due to

https://dx.doi.org/10.1021/acsaelm.0c00876
ACS Appl. Electron. Mater. 2021, 3, 170−175

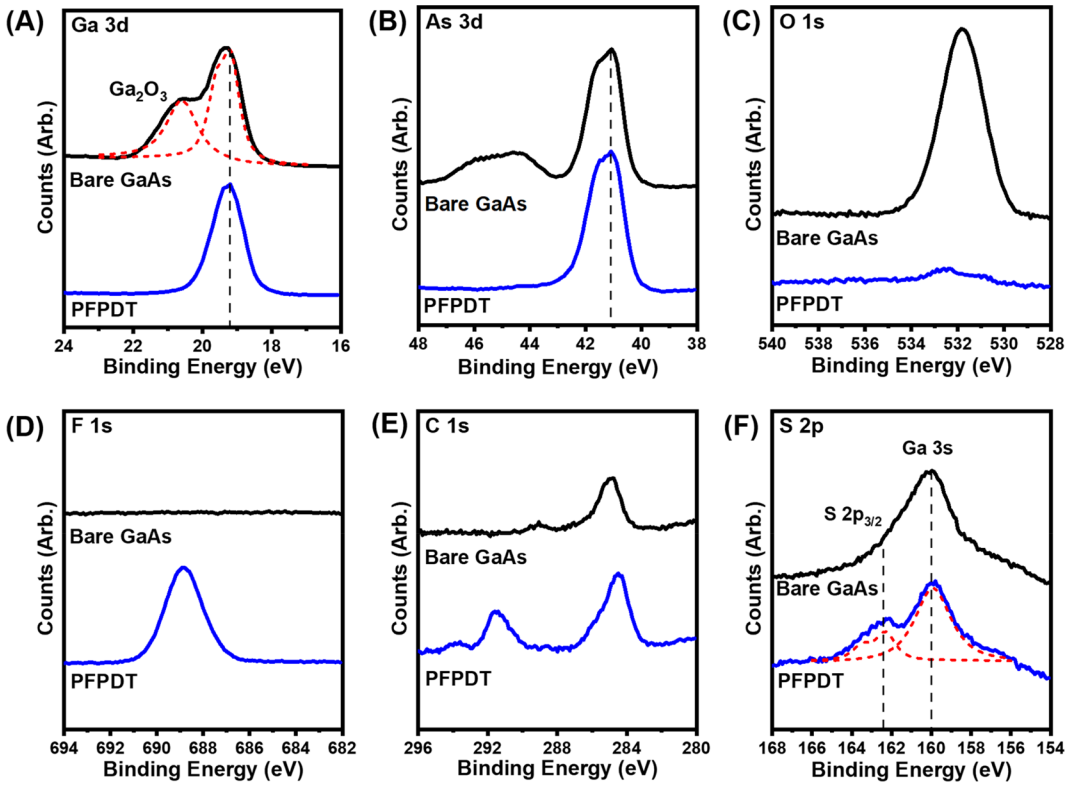

Figure 1. XPS spectra of the (A) Ga 3d, (B) As 3d, (C) O 1s, (D) F 1s, (E) C 1s, and (F) S 2p binding regions of the bare GaAs and PFPDT-printed GaAs(100) surface. The red dashed lines represent deconvoluted peaks. The GaAs surface was exposed to ambient conditions for 30 min. The XPS instrument was equipped with an Al Kα X-ray source ($h\nu$ = 1486.7 eV) and takeoff angle from the surface fixed at 45°.

Table 1. Peak Assignment and Binding Energies (eV) from XPS Spectra of the Bare GaAs and PFPDT-Printed GaAs(100) Surfaces

		binding energy (eV)		
binding region	assignment	bare GaAs	PFPDT SAM	reference[a]
Ga 3d	gallium oxides	20.6		>19.8
	Ga $3d_{5/2}$ (GaAs)	19.3	19.3	19.2 ± 0.04
As 3d	arsenic oxides	>43.0		>43.0
	As $3d_{5/2}$ (GaAs)	41.1	41.1	41.1 ± 0.04
C 1s	carbon contaminant	284.8		284.8
	CF_3		293.4	
	CF_2		291.4	
	CH_2		284.5	
F 1s	F in PFPDT		688.9	
S 2p	Ga 3s	160.0	160.0	160.0 ± 0.07
	S $2p_{1/2}$		163.4	
	S $2p_{3/2}$		162.3	162.4 ± 0.1
O 1s	GaAs oxides	531.9		532.0 ± 0.04
	O in PFPDT		532.7	

[a]The listed values were obtained from refs 21−27.

the fluorocarbons on the adsorbate, which are absent on the bare GaAs surface. In Figure 1E, there is a small peak from ambient hydrocarbon contamination in the C 1s region for the bare GaAs at 284.8 eV that is not present in the PFPDT-printed surface.[26] On the other hand, the three peaks in the spectrum of the PFPDT-printed surface can be attributed to the PFPDT adsorbate on the surface; specifically, the peaks at 293.4, 291.4, and 284.5 eV are attributed to the CF_3, CF_2, CH_2, and carbons of the phenyl ring, respectively.[18] Finally, the spectra in the S 2p region in Figure 1F was used to evaluate the binding of the thiol headgroup on the GaAs surface. The overlapping Ga 3s peak at 160.0 eV[27] complicates the evaluation of the binding; however, peak deconvolution (red line in Figure 1F) reveals a doublet that can be attributed to S $2p_{1/2}$ (~163.4 eV) and S $2p_{3/2}$ (~162.3 eV), which are characteristic of a bound thiolate on GaAs.[14,24]

Ellipsometric Thickness and Contact Angle Measurements. To confirm the formation of the monolayer and evaluate its interfacial properties, we characterized the GaAs substrate by ellipsometry before and after removal of the oxide layer as well as after printing with the PFPDT SAM. As shown by the ellipsometry data in Table 2, the PFPDT adsorbate produces a SAM that is 14 Å thick, even with a short deposition time of 1 min. Although the monolayer is thinner than the corresponding SAM on Au (24 Å) after 48 h of incubation,[20] the monolayer on GaAs produces a hydrophobic and oleophobic film (see Table 2 and Figure S1). To demonstrate the interfacial properties of the μCP-SAM, we

Table 2. Ellipsometric Thickness of the PFPDT SAM, Advancing Contact Angles of Water and Diiodomethane on the Investigated Surfaces, and Surface Energies of the Investigated Surfaces

surface	SAM thickness (Å)	water (θ_a, deg)	CH_2I_2 (θ_a, deg)	surface energy (mJ/m^2)
GaAs with oxide		76 ± 2	45 ± 2	40 ± 1
GaAs without oxide		39 ± 2	27 ± 2	63 ± 1
PFPDT SAM	14 ± 1	116 ± 2	80 ± 2	18 ± 1

https://dx.doi.org/10.1021/acsaelm.0c00876
ACS Appl. Electron. Mater. 2021, 3, 170−175

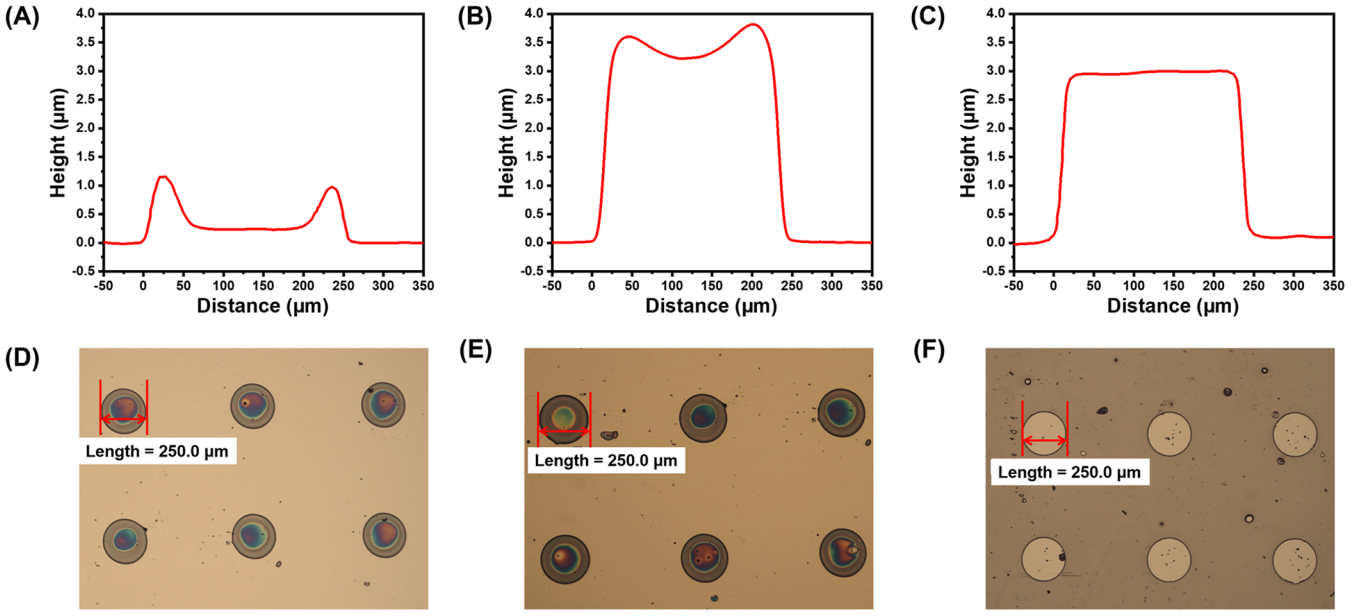

Figure 2. Cross-section profiles for mesa with a diameter = 250.0 μm atop GaAs with corresponding microscope images (A, (D) before etching, (B, E) after etching, and (C, F) after etching and resin removal.

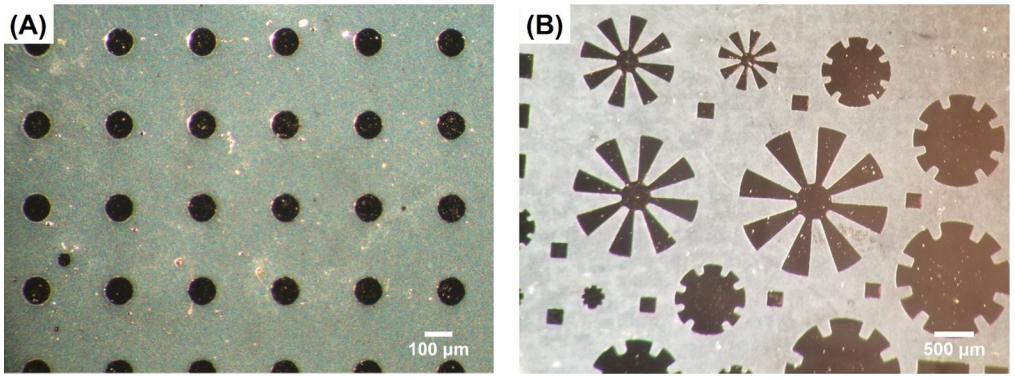

Figure 3. Microscope images of (A) mesas with a diameter of 100 μm and (B) microstructures on GaAs of different sizes and shapes.

measured advancing contact angles using water and diiodomethane, and the surface energies were calculated by using the Owens–Wendt method (see Table 2).[28]

The contact angle data in Table 2 show that the bare GaAs surface with and without the oxide layer are hydrophilic, with water contact angles of 76° and 39°, respectively, in contrast with the PFPDT-printed substrate (water contact angle of 116°). A similar trend was observed with regard to oleophobicity with diiodomethane as the contacting liquid, which gave contact angles of 45°, 63°, and 80° for the GaAs with oxide, without oxide, and PFPDT-printed substrate, respectively.

Moreover, the GaAs(100) surface with a native oxide layer exhibited a surface energy of 40 mJ/m^2, which increased by more than 50% (to 63 mJ/m^2) after etching of the oxide layer. In contrast, printing of PFPDT on the GaAs surface lowered the surface energy to 18 mJ/m^2, which is comparable to that of PTFE (18–19 mJ/m^2).[19,29] The drastically different surface energies of the PFPDT-printed and bare GaAs substrate (without the oxide layer) are the driving force for the spontaneous dewetting of the PFPDT-printed areas in our method. Importantly, analogous efforts to apply the reverse patterning process using commercially available monodentate thiols, such as octadecanethiol or 1*H*,1*H*,2*H*,2*H*-perfluoro-1-hexanethiol, failed to produce resin-resistant SAMs using the same stamping time (60 s) as the bidentate PFPDT adsorbate, which led to an incomplete pattern transfer in the former cases. We also note that dewetting is also a function of the surface tension and adhesive behavior of the phenolic resin on the GaAs surface. We found that a 10% w/w phenolic resin in methoxypropyl acetate in combination with the PFPDT-printed SAM exhibited the best results for creating clear patterns on GaAs by dip coating (vide infra).

Analysis of the Lithography Results. After printing the SAM onto the GaAs surface, deposition of the resin, and subsequent annealing at 120 °C for 5 min, the solvent in the resin solution evaporated to give a hard resin pattern. Figure 2 shows cross-section profiles and microscope images of the PFPDT-printed GaAs surface after steps 4–6 of the RPL process using a mesa with a diameter of 250.0 μm as a representative example. The cross-section profile shown in Figure 2A depicts a mesa with a thickness of 0.20 ± 0.05 μm in the center. The edges exhibited a greater thickness (additional 0.80 ± 0.05 μm) compared to the center region due to a coffee-ring effect (Figure 2D) arising from the stamping method.[30] Regardless of the disparate resin deposition, Figure

https://dx.doi.org/10.1021/acsaelm.0c00876
ACS Appl. Electron. Mater. 2021, 3, 170–175

2B shows that sharp-edges are obtained after etching with the resin remaining unchanged at the top (Figure 2E). Furthermore, after removal of the resin in the final step, the mesa on the GaAs substrate exhibited clear edges with minimal defects, as shown in Figures 2C and 2F.

The mesas can reach a thickness of 3.0 μm in 10 min, depending on the morphology of the GaAs material and wet etching time. The above results indicate that the phenolic resin acts as a wet-etching resist that is stable in etching solution (i.e., dilute hydrogen peroxide/sulfuric acid) and protects the GaAs surface underneath. The SAM-coated area, on the other hand, is etched because of the oxidizable sulfur groups bound to the GaAs surface. Here, we note a similar etching speed for the SAM-printed GaAs areas as the bare GaAs, which indicates that the SAM layer decomposes within 1 min in the etching solution. However, we note that longer etching times in efforts to obtain mesas thicker than 3.0 μm lead to deformed edges due to the thinness of the resin as well as the isotropic etching effect of the etching solution.

To determine the resolution of the RPL method, we reduced the diameter of the mesa. As shown in Figure 3A, mesas in total with diameters of 100.0 μm were obtained on GaAs with minimal defects following the RPL method. Attempts to decrease the diameter of the mesa further led to incomplete mesas, limiting the RPL method to structures with diameters of 100.0 μm. In addition to obtaining mesas with a minimum diameter of 100.0 μm, the RPL method can also be used for the large-scale production of mesas on GaAs; ~400 mesas were obtained per stamp. To evaluate the versatility of the RPL method, we produced stamps with various shapes and sizes. Figure 3B shows the generated structures with sharp edges ranging in size from 200 to 1500 μm.

In summary, we developed a new microstructuring method for GaAs substrates, reverse patterning lithography (RPL), as an alternative to conventional photolithography. Ellipsometric data and contact angle measurements of the PFPDT-printed GaAs surfaces show a 14 Å thick hydrophobic and oleophobic SAM, which significantly decreased the surface energy of the original oxide-free GaAs surface. Analysis of the printed SAM by XPS showed that the PFPDT adsorbate binds chemically to the GaAs surface and prevents its facile reoxidation. Studies using the RPL patterning method illustrated positive pattern formation on GaAs wafers using various designed shapes. The patterns obtained by the RPL method can reach a diameter of 100.0 μm with a depth of up to 3.0 μm thick by wet etching. These results not only validate the feasibility of the RPL method for the formation of microstructures on GaAs substrates but also provide a new paradigm for microstructuring GaAs substrates that warrants further investigation for the large-scale manufacturing of GaAs-based devices, with particular relevance for transistors and solar cells.

■ ASSOCIATED CONTENT

Supporting Information

The Supporting Information is available free of charge at https://pubs.acs.org/doi/10.1021/acsaelm.0c00876.

A list of materials, the procedure used for the fabrication of the polydimethylsiloxane (PDMS) stamps, and in-depth descriptions of the methods used to characterize the substrates (PDF)

■ AUTHOR INFORMATION

Corresponding Authors

T. Randall Lee − *Department of Chemistry, the Texas Center for Superconductivity, and the Advanced Manufacturing Institute, University of Houston, Houston, Texas 77204-5003, United States;* orcid.org/0000-0001-9584-8861; Email: trlee@uh.edu

Venkat Selvamanickam − *Department of Mechanical Engineering, the Texas Center for Superconductivity, and the Advanced Manufacturing Institute, University of Houston, Houston, Texas 77204-4006, United States*; Email: selva@uh.edu

Authors

Tianlang Yu − *Department of Chemistry, the Texas Center for Superconductivity, and the Advanced Manufacturing Institute, University of Houston, Houston, Texas 77204-5003, United States;* orcid.org/0000-0001-6218-5694

Devendra Khatiwada − *Department of Mechanical Engineering, the Texas Center for Superconductivity, and the Advanced Manufacturing Institute, University of Houston, Houston, Texas 77204-4006, United States*

Sahil Sharma − *Department of Mechanical Engineering, the Texas Center for Superconductivity, and the Advanced Manufacturing Institute, University of Houston, Houston, Texas 77204-4006, United States*

Maria D. Marquez − *Department of Chemistry, the Texas Center for Superconductivity, and the Advanced Manufacturing Institute, University of Houston, Houston, Texas 77204-5003, United States*

Complete contact information is available at: https://pubs.acs.org/10.1021/acsaelm.0c00876

Notes

The authors declare no competing financial interest.

■ ACKNOWLEDGMENTS

We thank the National Science Foundation (CHE-1710561), the Robert A Welch Foundation (Grant E-1320), the Texas Center for Superconductivity at the University of Houston, and the Advanced Manufacturing Institute at the University of Houston for generous support of this research.

■ REFERENCES

(1) Nagatsuma, T.; Kasamatsu, A. In *Terahertz Communications for Space Applications*, 2018 Asia-Pacific Microwave Conference (APMC), 6−9 Nov 2018; pp 73−75.

(2) Camarchia, V.; Pirola, M.; Quaglia, R.; Jee, S.; Cho, Y.; Kim, B. The Doherty Power Amplifier: Review of Recent Solutions and Trends. *IEEE Trans. Microwave Theory Technol.* **2015**, *63*, 559−571.

(3) Ye, P. D.; Wilk, G. D.; Yang, B.; Kwo, J.; Chu, S. N. G.; Nakahara, S.; Gossmann, H. J. L.; Mannaerts, J. P.; Hong, M.; Ng, K. K.; Bude, J. GaAs metal−oxide−semiconductor field-effect transistor with nanometer-thin dielectric grown by atomic layer deposition. *Appl. Phys. Lett.* **2003**, *83*, 180−182.

(4) Yoon, J.; Jo, S.; Chun, I. S.; Jung, I.; Kim, H. S.; Meitl, M.; Menard, E.; Li, X.; Coleman, J. J.; Paik, U.; Rogers, J. A. GaAs photovoltaics and optoelectronics using releasable multilayer epitaxial assemblies. *Nature* **2010**, *465*, 329−333.

(5) Green, M. A.; Hishikawa, Y.; Dunlop, E. D.; Levi, D. H.; Hohl-Ebinger, J.; Ho-Baillie, A. W. Y. Solar cell efficiency tables (version 51). *Prog. Photovoltaics* **2018**, *26*, 3−12.

(6) Chen, W.; Wang, Z.; Chen, X.; Zhang, S. Radio frequency power amplifier for wireless communication. In *Microwave Wireless Communications*, 2016; pp 261−300.
(7) Liu, i.; Ma, K.; Mou, S.; Meng, F. A review of recent power amplifier IC. In *2017 10th Global Symposium on Millimeter-Waves*, 2017; pp 87−91.
(8) Asadirad, M.; Rathi, M.; Pouladi, S.; Yao, Y.; Dutta, P.; Shervin, S.; Lee, K. H.; Zheng, N.; Ahrenkiel, P.; Selvamanickam, V.; Ryou, J.-H. III-V thin-film photovoltaic solar cells based on single-crystal-like GaAs grown on flexible metal tapes. In *2016 IEEE 43rd Photovoltaic Specialists Conference (PVSC)*; IEEE: Portland, OR, 2016; pp 1954−1956.
(9) Pouladi, S.; Rathi, M.; Khatiwada, D.; Asadirad, M.; Oh, S. K.; Dutta, P.; Yao, Y.; Gao, Y.; Sun, S.; Li, Y.; Shervin, S.; Lee, K.-H.; Selvamanickam, V.; Ryou, J.-H. High-efficiency flexible III-V photovoltaic solar cells based on single-crystal-like thin films directly grown on metallic tapes. *Prog. Photovoltaics* **2019**, *27*, 30−36.
(10) Seisyan, R. P. Nanolithography in microelectronics: A review. *Technol. Phys.* **2011**, *56*, 1061−1073.
(11) Chen, Y. Applications of nanoimprint lithography/hot embossing: a review. *Appl. Phys. A: Mater. Sci. Process.* **2015**, *121*, 451−465.
(12) Qin, D.; Xia, Y.; Whitesides, G. M. Soft lithography for micro- and nanoscale patterning. *Nat. Protoc.* **2010**, *5*, 491−502.
(13) Kao, P. C.; Chu, S. Y.; Chen, T. Y.; Zhan, C. Y.; Hong, F. C.; Chang, C. Y.; Hsu, L. C.; Liao, W. C.; Hon, M. H. Fabrication of Large-Scaled Organic Light Emitting Devices on the Flexible Substrates Using Low-Pressure Imprinting Lithography. *IEEE Trans. Electron Devices* **2005**, *52*, 1722−1726.
(14) Mancheno-Posso, P.; Muscat, A. J. Self-assembly of alkanethiolates directs sulfur bonding with GaAs(100). *Appl. Surf. Sci.* **2017**, *397*, 1−12.
(15) Sheen, C. W.; Shi, J. X.; Maartensson, J.; Parikh, A. N.; Allara, D. L. A new class of organized self-assembled monolayers: alkanethiols on gallium arsenide(100). *J. Am. Chem. Soc.* **1992**, *114*, 1514−1515.
(16) Srisombat, L.; Jamison, A. C.; Lee, T. R. Stability: A key issue for self-assembled monolayers on gold as thin-film coatings and nanoparticle protectants. *Colloids Surf., A* **2011**, *390*, 1−19.
(17) Chinwangso, P.; Jamison, A. C.; Lee, T. R. Multidentate adsorbates for self-assembled monolayer films. *Acc. Chem. Res.* **2011**, *44*, 511−519.
(18) Rittikulsittichai, S.; Park, C. S.; Marquez, M. D.; Jamison, A. C.; Frank, T.; Wu, C. H.; Wu, J. I.; Lee, T. R. Inhibiting Reductive Elimination as an Intramolecular Disulfide Dramatically Enhances the Thermal Stability of SAMs on Gold Derived from Bidentate Adsorbents. *Langmuir* **2018**, *34*, 6645−6652.
(19) Lee, S.; Park, J. S.; Lee, T. R. The wettability of fluoropolymer surfaces: influence of surface dipoles. *Langmuir* **2008**, *24*, 4817−4826.
(20) Lee, H. J.; Jamison, A. C.; Lee, T. R. Two Are Better than One: Bidentate Adsorbates Offer Precise Control of Interfacial Composition and Properties. *Chem. Mater.* **2016**, *28*, 5356−5364.
(21) Lu, H.; Kind, M.; Terfort, A.; Zharnikov, M. Structure of Self-Assembled Monolayers of Partially Fluorinated Alkanethiols on GaAs(001) Substrates. *J. Phys. Chem. C* **2013**, *117*, 26166−26178.
(22) Lu, H.; Zharnikov, M. Structure-Building Forces in Biphenyl-Substituted Alkanethiolate Self-Assembled Monolayers on GaAs(001): The Effect of the Bending Potential. *J. Phys. Chem. C* **2015**, *119*, 27401−27409.
(23) Shaporenko, A.; Adlkofer, K.; Johansson, L. S. O.; Ulman, A.; Grunze, M.; Tanaka, M.; Zharnikov, M. Spectroscopic Characterization of 4'-Substituted Aromatic Self-Assembled Monolayers on GaAs(100) Surface. *J. Phys. Chem. B* **2004**, *108*, 17964−17972.
(24) Moulder, J. F.; Chastain, J.; Sobol, P. E.; Bomben, K. D. *Handbook of X-ray Photoelectron Spectroscopy*; Perkin-Elmer: Eden Prairie, MN, 1992.
(25) Shaporenko, A.; Adlkofer, K.; Johansson, L. S. O.; Tanaka, M.; Zharnikov, M. Functionalization of GaAs Surfaces with Aromatic Self-Assembled Monolayers: A Synchrotron-Based Spectroscopic Study. *Langmuir* **2003**, *19*, 4992−4998.
(26) McGuiness, C. L.; Shaporenko, A.; Mars, C. K.; Uppili, S.; Zharnikov, M.; Allara, D. L. Molecular self-assembly at bare semiconductor surfaces: preparation and characterization of highly organized octadecanethiolate monolayers on GaAs(001). *J. Am. Chem. Soc.* **2006**, *128*, 5231−5243.
(27) McGuiness, C. L.; Shaporenko, A.; Zharnikov, M.; Walker, A. V.; Allara, D. L. Molecular Self-Assembly at Bare Semiconductor Surfaces: Investigation of the Chemical and Electronic Properties of the Alkanethiolate−GaAs(001) Interface. *J. Phys. Chem. C* **2007**, *111*, 4226−4234.
(28) Rudawska, A.; Jacniacka, E. Analysis for determining surface free energy uncertainty by the Owen−Wendt method. *Int. J. Adhes. Adhes.* **2009**, *29*, 451−457.
(29) Yu, T.; Marquez, M. D.; Zenasni, O.; Lee, T. R. Mimicking Polymer Surfaces Using Cyclohexyl- and Perfluorocyclohexyl-Terminated Self-Assembled Monolayers. *Acs Appl. Nano Mater.* **2019**, *2*, 5809−5816.
(30) Seo, C.; Jang, D.; Chae, J.; Shin, S. Altering the coffee-ring effect by adding a surfactant-like viscous polymer solution. *Sci. Rep.* **2017**, *7*, 500.

https://dx.doi.org/10.1021/acsaelm.0c00876
ACS Appl. Electron. Mater. 2021, 3, 170−175